AFRL-AFOSR-JP-TR-2021-0005

Quantum photon manipulation and measurement with ultra-thin metasurfaces

Sukhorukov, Andrey
AUSTRALIAN NATIONAL UNIVERSITY RESEARCH OFFICE ACTON (AUSTRALIA)
10C EAST RD
ACTON, ,
AU

07/26/2021
Final Technical Report

Air Force Research Laboratory
Air Force Office of Scientific Research
Asian Office of Aerospace Research and Development
Unit 45002, APO AP 96338-5002

REPORT DOCUMENTATION PAGE

Form Approved
OMB No. 0704-0188

1. REPORT DATE *(DD-MM-YYYY)*	**2. REPORT TYPE**	**3. DATES COVERED** *(From - To)*
26-07-2021	Final	22 Jul 2019 - 22 Oct 2020

4. TITLE AND SUBTITLE
Quantum photon manipulation and measurement with ultra-thin metasurfaces

5a. CONTRACT NUMBER
FA2386-19-1-4053

5b. GRANT NUMBER

5c. PROGRAM ELEMENT NUMBER

6. AUTHOR(S)
Andrey Sukhorukov

5d. PROJECT NUMBER

5e. TASK NUMBER

5f. WORK UNIT NUMBER

7. PERFORMING ORGANIZATION NAME(S) AND ADDRESS(ES)
AUSTRALIAN NATIONAL UNIVERSITY RESEARCH OFFICE ACTON (AUSTRALIA)
10C EAST RD
ACTON,
AU

8. PERFORMING ORGANIZATION REPORT NUMBER

9. SPONSORING/MONITORING AGENCY NAME(S) AND ADDRESS(ES)
AOARD
UNIT 45002
APO AP 96338-5002

10. SPONSOR/MONITOR'S ACRONYM(S)
AFRL/AFOSR IOA

11. SPONSOR/MONITOR'S REPORT NUMBER(S)
AFRL-AFOSR-JP-TR-2021-0005

12. DISTRIBUTION/AVAILABILITY STATEMENT
A Distribution Unlimited: PB Public Release

13. SUPPLEMENTARY NOTES

14. ABSTRACT
See attached report

15. SUBJECT TERMS

16. SECURITY CLASSIFICATION OF:			**17. LIMITATION OF ABSTRACT**	**18. NUMBER OF PAGES**	**19a. NAME OF RESPONSIBLE PERSON**
a. REPORT	**b. ABSTRACT**	**c. THIS PAGE**			CHRISTOPHER VERGIEN
U	U	U	SAR	17	**19b. TELEPHONE NUMBER** *(Include area code)* 315-227-7002

Annual Report for AOARD Grant 19IOA053

"**Quantum photon manipulation and measurement with ultra-thin metasurfaces**"

Date: 15 January 2020

Name of Principal Investigators (PI and Co-PIs): Prof. Andrey Sukhorukov

- e-mail address : andrey.sukhorukov@anu.edu.au
- Institution : Australian National University
- Mailing Address : Nonlinear Physics Centre, Research School of Physics, Australian National University, Canberra, ACT 2601, Australia
- Phone : +61-2-6125-8276
- Fax : +61-2-6125-8588

Period of Performance: 07/23/2019 – 10/22/2020

Abstract:
The project developed ultra-thin optical metasurfaces for flexible control of the quantum photon polarization states in unconventional regimes. The key advantage of this platform is that the parallel photon interference in nano-resonator arrays enables ultimate miniaturization, in contrast to sequential interference stages in conventional quantum circuits. We have designed metasurfaces with binary nano-resonator arrays that realize simultaneous polarization manipulation and filtering, operating across the telecommunication wavelengths. The metasurfaces can implement arbitrary polarization transformations of entangled photon pairs, and in particular can change the degree of quantum entanglement. We fabricated the metasurfaces on a dielectric platform without material absorption and demonstrated their high efficiency in experiments. Such ultra-thin meta-devices can find applications in quantum network components. Furthermore, we found that the metasurfaces can enable discrimination of polarization objects, with possible applications from microscopy to monitoring of network links. We also developed new efficient approaches for one-shot multi-photon polarization state measurement with a single metagrating even in presence of fabrication imperfections, and for monitoring deviations from a target polarization state. The latter results can facilitate diverse applications demanding quantum state characterization.

Introduction:

Manipulation and measurement of quantum photon states are essential capabilities for the realization of quantum networks, including fiber-based and free-space communications. Traditionally, this is performed through multiple stages of photon shaping and interference, implemented with bulk optical components or extended waveguides. However, such approaches require precise alignment, being sensitive to the environmental instabilities, such as vibrations and temperature variations. The research objective is to develop a new fundamental approach based on ultra-thin all-dielectric metasurfaces, where a single nano-layer encodes multiple parallel quantum state transformations. This platform can achieve the ultimate miniaturization and stability combined with high accuracy and robustness, while overcoming the limitations of lengthy sequential implementations. The project objective is to develop the capability of metasurfaces for flexible control of the quantum photon polarization state in unconventional regimes. The technical approach is based on special design of metasurfaces which can act as ultra-compact and stable complex polarization waveplates, which simultaneously perform polarization transformation and filtering. This will drive the future development of ultra-thin metasurfaces providing advanced functionalities in photon state shaping, imaging, and measurement for applications in diverse quantum communication networks.

Experiment:

Arbitrary transformation of polarization photon pairs. The corresponding theoretical and experimental

approaches are fully described in the journal paper [1]. In the following, we provide a summary of key aspects of this work.

A new regime of the so-called complex birefringence has recently been suggested, extending the notion of real-valued birefringence. The presence of tailored polarization-dependent loss can enable fundamentally new possibilities for polarization control, which cannot be achieved with conventionally birefringent media alone. For example, complex birefringent structures could be used to change the angle between a pair of polarization states, as illustrated in Fig. 1.1. As shown, a pair of nearby polarization vectors can become orthogonal after propagating in the complex-birefringent medium, whereas in conventional birefringence the relative angle remains constant.

We developed a new theoretical approach for implementing complex birefringence with all-dielectric metasurfaces, without material gain or absorption. We formulate a practical design principle that is optimal for achieving any desirable polarization transformation with a minimum amount of loss, which is realized through judiciously engineered polarization-dependent diffraction [Fig. 1.2]. Such loss can be effectively eliminated for certain polarization states, presenting a fundamental advantage compared to the material loss exhibited by all states in plasmonic structures. Our approach can be tailored for arbitrary polarization pairs along with polarization transformation and phase control, which can underpin a new generation of polarization optical devices for classical and quantum applications.

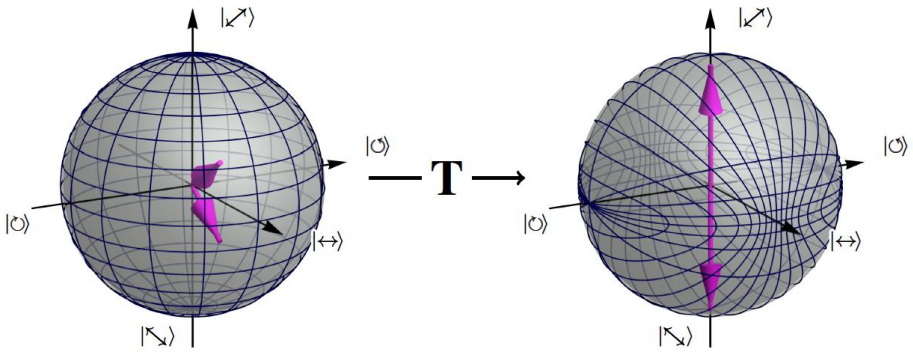

Figure 1.1: Transformation of polarization states with a complex-birefringent wave plate, visualized on a Poincaré sphere. Left: two input states with close polarization state vectors indicated by purple arrows. Right: state vectors (purple arrows) after a transmission via a complex-birefringent wave plate, which become orthogonal. Gridlines on the surfaces illustrate the transformations for other states.

We then perform detailed numerical modeling to design the binary metasurfaces with various transmission characteristics. The structures were tailored for operation at the wavelength of $\lambda_0 = 1550\text{nm}$, within the range of the telecommunications band. The nanoresonators are placed on a square lattice. We selected the structure period as $d = 1800\text{nm}$, which satisfies the following requirement: **(i)** $d > \lambda_0$ to allow diffraction, which acts as polarization-dependent loss, and **(ii)** nano-resonators are positioned sufficiently close to suppress direct light transmission through the substrate. We consider resonators in the form of rectangular cuboids made of amorphous-silicon on a glass substrate, and achieve control of transmission phase along the extraordinary and ordinary axes (ϕ_e and ϕ_o) by modifying their physical dimensions (L_e, L_o) in the plane of the metasurface. These dimensions are determined by numerical simulations.

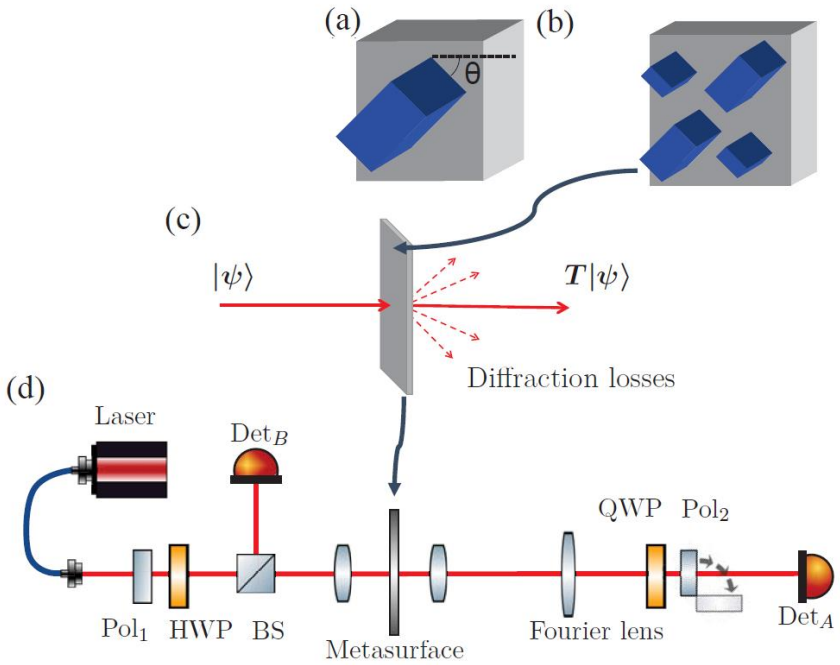

Figure 1.2: Concept of realizing complex birefringence with all-dielectric metasurfaces. (a) A single-structure unit cell with dielectric nano-pillar placed at an angle θ realizing real birefringence, with real-valued phase retardation along the two principal axes. (b) A unit cell with two pairs of distinctly sized nano-pillars realizing complex birefringence. (c) A metasurface utilizing the unit cell in (b), realizing engineered polarization-dependent losses via diffraction. (d) Schematic diagram of the experimental setup utilized to characterize the manufactured samples.

The nanostructures were fabricated on a 710-nm-thick amorphous-silicon thin film prepared using Plasma-Enhanced Chemical Vapor Deposition (PECVD) on a $170\mu m$ thick glass substrate. Then, etching was carried out via Electron Beam Lithography (EBL) and Inductively Coupled Plasma (ICP) etching. Varying exposures (from approximately $150\mu Ccm^{-2}$ to $200\mu Ccm^{-2}$) were utilized to produce a small range of metasurfaces with slight variations in sizes to account for fabrication variances. The fabricated metasurfaces were characterized using a variable-wavelength laser operating in the $1500-1575nm$ telecommunication range as the light source [Fig. 1.2(d)], and input polarization states were prepared from this laser using a fixed linear polarizer (Pol_1) and a motorized half-wave plate (HWP). A 50:50 beam splitter (BS) and detector were introduced immediately after the state preparation to provide a normalization baseline for the measurements. A lens focused the beam to an approximate $80\mu m$ spot normally incident on the metasurface, followed by an objective lens used to image the transmitted light. To exclusively collect zero-th order transmitted light, a Fourier lens was used to exclude higher orders of diffracted light. Then, the polarization was characterized via a motorized quarter-wave plate (QWP) and a linear polarizer (Pol_2) to project the transmitted state onto a varying basis for reconstruction.

We reveal the capability for arbitrary transformation of quantum biphoton polarization states with complex birefringent metasurfaces, as sketched in Fig. 1.3(a). We note that any pure state of two polarization-entangled photons can be expressed as

$$|\Psi(A,B)\rangle = \frac{a^\dagger(A)a^\dagger(B)|0\rangle}{||a^\dagger(A)a^\dagger(B)|0\rangle||},$$

where A and B are two single-photon polarization states, and $a^\dagger$ is a one-photon creation operator. This expression means that a quantum two-photon state can be represented by a pair of points on the Poincaré sphere, for example such as those indicated by two arrows in Fig. 1.1(a).

The action of the metasurface on a two-photon state will, in general, produce a superposition of pure two-photon and mixed single-photon (when a paired photon is lost) states, which can be distinguished through conditional detection schemes. The two-photon state transformation is simply expressed as:

$$|\Psi(A_i, B_i)\rangle \xrightarrow{T} |\Psi(TA_i, TB_i)\rangle = |\Psi(A_t, B_t)\rangle.$$

This means that we can apply the approaches formulated above for the simultaneous independent transformation of a pair of polarization states. Importantly, the capacity of a complex birefringent metasurface to change the angle between the pair of states on a Poincaré sphere, such as illustrated in Fig. 1.1, enables the modification of the degree of quantum entanglement, which would be impossible with conventional conservative birefringence. Thereby, a transformation between arbitrary selected input to output quantum two-photon states can be accomplished.

Next, we showcase an experimental potential for tailored two-photon manipulation and quantum state transformation. Recent studies demonstrated that photon interference in lossy couplers can demonstrate unconventional features, including a transition between bunching and anti-bunching statistics. The previous experiments were based on plasmonic structures with inherently high metal absorption. Here, we present a new design of all-dielectric metasurface which realizes a non-conservative coupler with the minimum necessary amount of loss. Specifically, we consider the coupling transformation between the $|H\rangle$ and $|V\rangle$ polarizations with a non-conservative transfer matrix in the form:

$$T_\varphi = \rho \begin{bmatrix} 1 & e^{i\varphi} \\ e^{i\varphi} & 1 \end{bmatrix},$$

where ρ is a scaling coefficient. The phase value of $\varphi = \pi/2$ corresponds to a conventional conservative coupler, while other phases generally correspond to non-conservative transformations. The optimal practical realization with the minimal necessary amount of losses in structures without gain corresponds to the maximum possible value of ρ, which is achieved when the maximum singular value of the transfer matrix $\sigma_1 \to 1$.

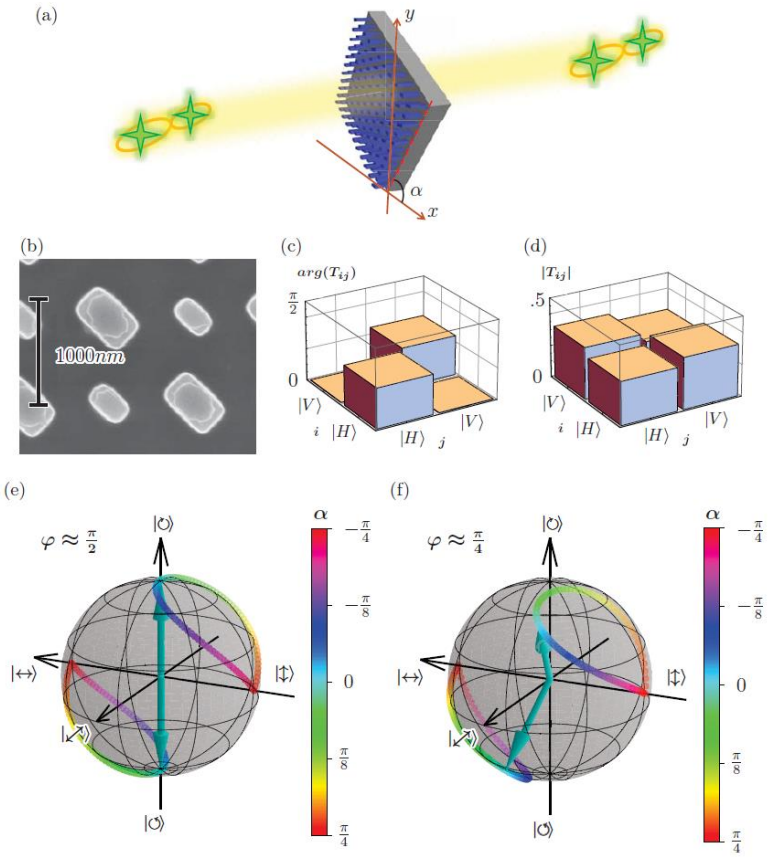

Figure 1.3: Application of complex-birefringent metasurfaces for arbitrary transformation of polarization-entangled two photon states. (a) Schematic of a metasurface oriented at an angle α to perform the desired transformation for entangled photon pairs. (b) SEM image of a metasurface made of amorphous-silicon on a glass substrate. (c,d) Experimentally characterized transfer matrix at a wavelength of 1560nm, including (c) arguments and (d) modulus of the elements. (e,f) Transformation of $|\Psi(H,V)\rangle$ entangled input state (e) by an ideal phase retarder rotated at angle α and (f) calculated

with the experimental transfer matrix of the metasurface oriented at angle α as shown in (a).

The general approach to complex birefringence formulated above enables us to design the binary metasurfaces which can realize the unconventional polarization coupling for arbitrary phase φ. We present an example of fabricated metasurface in Fig. 1.3(b), which transfer matrix [Figs. 1.3(c) and (d)] realizes the case of $\varphi \simeq \pi/4$. There is only a slight variation of the absolute values in the experimental transfer matrix, which still enables unconventional interference and control of the biphoton states.

We use the experimentally determined transfer matrix [Fig. 1.3(c) and (d)] to simulate the transformation of the input quantum state composed of orthogonally polarized entangled photons, $|\Psi(H,V)\rangle$, that is $A_i = H, B_i = V$. We further note that a rotation of a metasurface in the plane by angle α, as sketched in Fig. 1.3(a), nontrivially modifies the transformation as $R(\alpha)T_\varphi R(-\alpha)$ and thus the output states A_t and B_t. We visualize the output two-photon state by a pair of same-color points on the Poincaré sphere in Fig. 1.3(f), where the colors correspond to different metasurface orientation angles α and the arrows point to the output state at $\alpha = 0$. For comparison, we plot in Fig. 1.3(e) the output states which would be produced by a conventional conservative coupler with $\varphi = \pi/2$. We observe that in the conservative regime, the relative angle between the photon pairs is unchanged for all α [Fig. 1.3(e)], meaning that the degree of quantum entanglement at the output remains the same as at the input, in agreement with the properties of unitary operators. In contrast, this limitation is removed in the regime of complex birefringence, and the tailored change of relative angle [Fig. 1.3(f)] enables flexible entanglement control.

2) Discerning Polarization Objects using Non-local Measurements with Metasurfaces, Ref. [4].

We develop a protocol of quantum ghost polarimetry using polarization-entangled photons for the discrimination of fully or partially transparent polarization-sensitive elements of a known set. We show that entangled light is needed to discern all types of objects and we derive the object properties that entail the need for entanglement. Furthermore, we demonstrate that specific polarization transformations are needed for detection as conventional detectors are not sensitive to polarization. Our results reveal that specially designed highly transmissive dielectric metasurfaces are the most suitable implementation to map specific polarization states into detectable spatial patterns.

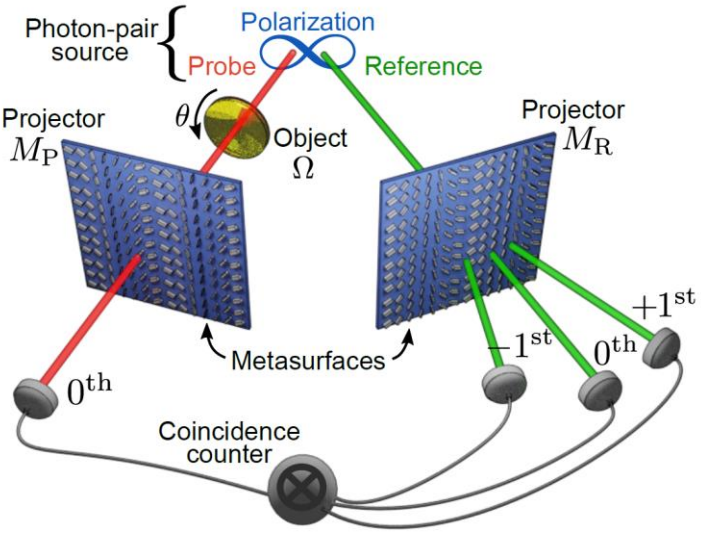

Figure 2.1: Sketch of the ghost polarimetry with metasurfaces.

Our proposed measurement scheme is depicted in Fig. 2.1. We consider a source that produces photon-pairs whose joint polarization state can be modeled by the following density matrix

$$\rho_{\text{in}} = \frac{1}{2}(|\text{H}_\text{P}\text{H}_\text{R}\rangle\langle\text{H}_\text{P}\text{H}_\text{R}| + |\text{V}_\text{P}\text{V}_\text{R}\rangle\langle\text{V}_\text{P}\text{V}_\text{R}|)$$
$$+q\left(\frac{1}{2}\right)(|\text{H}_\text{P}\text{H}_\text{R}\rangle\langle\text{V}_\text{P}\text{V}_\text{R}| + |\text{V}_\text{P}\text{V}_\text{R}\rangle\langle\text{H}_\text{P}\text{H}_\text{R}|),$$

with q representing the degree of entanglement, $0 \leq q \leq 1$, from the strongest classical correlation $q = 0$ to perfect entanglement $q = 1$. Throughout this manuscript, horizontal and vertical polarization are denoted H and V, respectively. The probe-photon interacts with an object Ω, which furthermore can be rotated by an angle θ, then is projected into a specific polarization state using the transformation M_P, and finally detected. After detection of the probe photon, the reduced state of the reference-photon is $\rho_\mathrm{R}{}' = \mathrm{tr}_\mathrm{P}[(T_\mathrm{P} \otimes 1)\, \rho_\mathrm{in}\, (T_\mathrm{P} \otimes 1)^\dagger]$, where $\mathrm{tr}_\mathrm{P}(\cdot)$ is the partial trace over the probe-photon and $T_\mathrm{P} = M_\mathrm{P}\Omega(\theta)$. The normalized reduced state of the reference-photon after measuring the probe-photon is then $\rho_\mathrm{R} = \rho_\mathrm{R}{}'/\mathrm{tr}(\rho_\mathrm{R}{}')$. The reference-photon does not interact with the object, but is projected onto several polarization bases by interacting with an optical element realizing the transformation M_R. We assume, that each of these polarization bases corresponds to a separate output channel, in which the probe photons then are detected using polarization-insensitive detectors. Whereas the measurements of the probe and reference photons alone do not allow to distinguish different objects Ω and their rotation angle θ, we will demonstrate that this is possible using coincidence measurements. The expectation value of the coincidence counts between the single output of projector M_P and the n-th output of projector M_R is $\langle n \rangle = tr\left[(M_{\mathrm{R},n})\rho_\mathrm{R}(M_{\mathrm{R},n})^\dagger\right]$. To distinguish objects, each projection basis $M_{\mathrm{R},n}$ in the reference arm is numerically engineered so that every reduced state ρ_R produces a distinctive pattern formed by a collection of n coincidence measurements.

The optimal choice of the probe-photon projector M_P can be investigated by geometrically representing the reduced state of the reference-photon ρ_R in the Poincaré spher, where each ρ_R is described by a vector $\mathbf{p} = [p_\mathrm{H}, p_\mathrm{D}, p_\mathrm{C}]$. Here, p_H corresponds to the degree of horizontal/vertical polarization, p_D to the diagonal/antidiagonal linear polarization at $\pm 45°$, and p_C to the right/left circular polarization. The Poincaré vector is found using the Pauli matrices X, Y, Z with $\mathbf{p} = [\mathrm{tr}(\rho_\mathrm{R} Z), \mathrm{tr}(\rho_\mathrm{R} X), -\mathrm{tr}(\rho_\mathrm{R} Y)]$. If the total transformation in the probe-arm, comprising the object Ω and projector M_P, is written in the basis of the photon-pair source as $T_\mathrm{P} = \sum T_{kl} |k\rangle\langle l|$ with $k, l \in \{\mathrm{H}, \mathrm{V}\}$, then

$$p_\mathrm{H} = \|T_\mathrm{P}\|_F^{-2}(|T_\mathrm{HH}|^2 + |T_\mathrm{VH}|^2 - |T_\mathrm{VV}|^2 - |T_\mathrm{HV}|^2),$$
$$p_\mathrm{D} = q\, \|T_\mathrm{P}\|_F^{-2}\mathrm{Re}(T_\mathrm{HH}T_\mathrm{HV}^* + T_\mathrm{VH}T_\mathrm{VV}^*),$$
$$p_\mathrm{C} = q\, \|T_\mathrm{P}\|_F^{-2}\mathrm{Im}(T_\mathrm{HH}T_\mathrm{HV}^* + T_\mathrm{VH}T_\mathrm{VV}^*),$$

where $\|\cdot\|_F$ is the Frobenius norm. Since we require that each object produces a different reduced state ρ_R, each ρ_R must occupy a unique position on or inside the Poincaré sphere.
The components of the Poincaré vector are connected as

$$p_\mathrm{H}^2 + \frac{p_\mathrm{D}^2 + p_\mathrm{C}^2}{q^2} = \left(\frac{\sigma_{1\mathrm{P}}^2 - \sigma_{2\mathrm{P}}^2}{\sigma_{1\mathrm{P}}^2 + \sigma_{2\mathrm{P}}^2}\right)^2,$$

where $\sigma_{1\mathrm{P}}$ and $\sigma_{2\mathrm{P}}$ are the singular values of the transformation T_P. This equation indicates that the reduced state of the reference-photon ρ_R obtained from the family of transformations T_P which have the same $|\sigma_{1\mathrm{P}}^2 - \sigma_{2\mathrm{P}}^2|/(\sigma_{1\mathrm{P}}^2 + \sigma_{2\mathrm{P}}^2)$, will lie on an ellipsoid of revolution of long axis $|\sigma_{1\mathrm{P}}^2 - \sigma_{2\mathrm{P}}^2|/(\sigma_{1\mathrm{P}}^2 + \sigma_{2\mathrm{P}}^2)$ and short axis $q|\sigma_{1\mathrm{P}}^2 - \sigma_{2\mathrm{P}}^2|/(\sigma_{1\mathrm{P}}^2 + \sigma_{2\mathrm{P}}^2)$ given that the degree of entanglement is in the range $0 \leq q \leq 1$. This ellipsoid reduces to a point, $p_\mathrm{H} = p_\mathrm{D} = p_\mathrm{C} = 0$, when $\sigma_{1\mathrm{P}} = \sigma_{2\mathrm{P}}$. Additionally, the ellipsoid is largest, for a fixed q, when one of the singular values is zero, $p_\mathrm{H}^2 + (p_\mathrm{D}^2 + p_\mathrm{C}^2)/q^2 = 1$. We concentrate on a scheme with a source of photon-pairs that have maximal entanglement $q = 1$, where the ellipsoid is a sphere with radius $|\sigma_{1\mathrm{P}}^2 - \sigma_{2\mathrm{P}}^2|/(\sigma_{1\mathrm{P}}^2 + \sigma_{2\mathrm{P}}^2)$.

The optimal projectors M_P and M_R in each arm of the setup can be found numerically. However, realizing these polarization transformations experimentally can be quite challenging, as they in general need to realize partial polarizers in elliptical bases, where the reference arm also needs several outputs. Here we demonstrate, that the projectors can be realized using nanostructured dielectric metasurfaces, which can effectively act as partial polarizers in arbitrary elliptical bases with any required extinction ratio [1]. Each metasurface is a flat optical element composed of a periodically repeated array of nano-resonators called meta-gratings. We perform optimization of the phase retardances and orientations associated with the individual nano-resonators to realize the required projectors. Specifically, we design a metasurface for the probe arm such that its zeroth diffraction order realizes the projector M_P. Similarly, a second metasurface is placed in the reference arm where the three outputs of projector M_R correspond to three diffraction orders (see Fig. 2.1). The unit-cell geometries of numerically found optimal meta-gratings for the considered set of objects $\Omega_{a,b,c}$ are depicted in Fig. 2.2(b).

We show in Fig. 2.2(c) the diffraction patterns of the objects $\Omega_{a,b,c}(\theta)$ represented in the space $\mathcal{D}$,

showcasing that the full identification of objects with their corresponding rotation angle is possible by optimizing the projectors M_{P} and M_{R}. The patterns in coincidences give non-zero photons counts since they lie on the plane $\langle -1\mathrm{st}\rangle + \langle 0\mathrm{th}\rangle + \langle +1\mathrm{st}\rangle \approx 0.8$ within space $\mathcal{D}$. As designed, the chosen three outputs of metasurface M_{R} map the geometric shape of Fig. 2.2(a, middle) into the space $\mathcal{D}$. This demonstrates that the full identification of objects with their corresponding rotation angle is possible by using optimized metasurfaces.

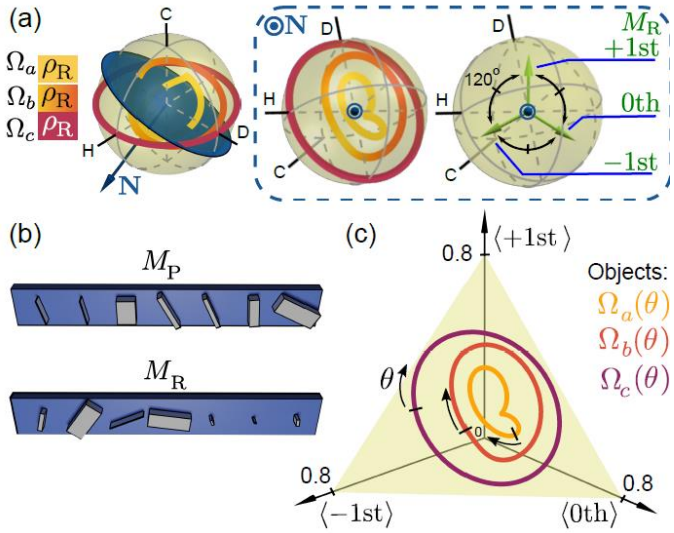

Figure 2.2: (a) Reduced state of the reference-photon ρ_{R} produced by a set of three objects $\Omega_{a,b,c}$ and an optimal metasurface M_{P} from two different perspectives. The vector $\mathbf{N}$ is normal to the blue plane where the optimal projection bases of the diffraction orders of the metasurface M_{R} are located. (b) Optimal meta-gratings in the probe M_{P} and reference M_{R} arms. (c) Diffraction patterns in coincidences for each of the objects $\Omega_{a,b,c}$ in the set, depicted in a space $\mathcal{D}$ where each diffraction order is a dimension, showing that the objects cannot only be discerned from one another but also their own rotation angle θ can be identified ($\theta = 0$ is marked with a small line, rotation symmetry is π).

3) Single Metagrating for Multi-Photon Polarization Measurements, Ref. [11].

We first formulate a general theory of polarization measurements. We consider a metasurface, which splits an input beam into several diffraction orders as sketched in Fig. 3.1(a). Then, the measurements of photon correlations between the output ports can be used to reconstruct the input quantum state. In previous studies, it was assumed that the photon polarization is specifically selected at each diffraction order. This effectively required the metasurface to act as a near-perfect polarization splitter, which came at a cost of larger device area requirements due to a need to interleave several gratings and the distortion of the output beam profile. In the following, we show that such limitation can be removed, allowing for a compact and robust metasurface design.

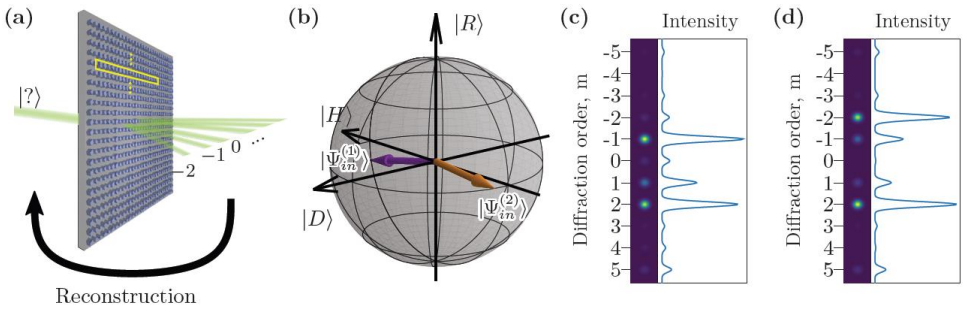

Figure 3.1: (a) Conceptual sketch of single-metagrating polarimetry. Highlighted in yellow is a single 16 resonator unit cell. From the output diffraction orders, any unknown input state may be reconstructed by knowing the metasurface instrument matrix. (b) Poincaré sphere representation of two arbitrarily

chosen input states $|\Psi_{in}^{(1)}\rangle$, $|\Psi_{in}^{(2)}\rangle$ characterized in Jones formalism by the polarization angles and phases (1.5,0.1), (0.1,1.5) respectively. (c,d) Intensities of output diffraction orders corresponding to the respective input states $|\Psi_{in}^{(1)}\rangle$, $|\Psi_{in}^{(2)}\rangle$.

Since we consider a linear regime, the transformation of quantum states can be expressed through the classical Jones transfer matrices $\mathbf{T}^{(m)}$ to of each diffraction orders number m,

$$\psi_{out}^{(m)} = \mathbf{T}^{(m)}\psi_{in} ,$$

where ψ_{in} and $\psi_{out}^{(m)}$ are the classical input and output polarization states at the respective diffraction orders. Each diffraction order functions, in general, as a partial polarizer acting on the incoming light. It is then convenient for the following analysis to perform a singular value decomposition (SVD) of the transfer matrices,

$$\mathbf{T}^{(m)} = U^{(m)}\, diag(s_{m,1}, s_{m,2})\, \left(W^{(m)}\right)^{\dagger} ,$$

where $s_{m,1}, s_{m,2} \geq 0$ are the singular values, $U^{(m)} = [U_1^{(m)}, U_2^{(m)}]$ and $W^{(m)} = [W_1^{(m)}, W_2^{(m)}]$ are unitary matrices, the subscripts indexing the respective columns. We choose the order of singular values such that $s_{m,1} \geq s_{m,2}$.

We note that if $s_{m,2} = 0$, the polarization state at the corresponding diffraction order is fixed as in a case of perfect polarizer. However in a general case of $s_{m,2} > 0$, the metasurface effectively acts as a partial polarizer, with the power extinction ratio of $(s_{m,2}/s_{m,1})^2$.

We now formulate the transformation by the metasurface of the photon creation and annihilation operators from the input, $\hat{a}_p^{\dagger}$ and $\hat{a}_p$, where $p = \{H, V\}$ is the polarization state, to each of the output diffraction orders, $\hat{b}_{m,p}^{\dagger}$ and $\hat{b}_{m,p}$. This can be expressed through the linear transfer matrix elements as:

$$\hat{b}_{m,p} = \sum_{p'=H,V} \left(\mathbf{T}_{p,p'}^{(m)}\right)^{*} \hat{a}_p \ , \quad \hat{b}_{m,p}^{\dagger} = \sum_{p'=H,V} \mathbf{T}_{p,p'}^{(m)}\, \hat{a}_p^{\dagger} \ . \qquad (3)$$

We target the tomography of quantum polarization-entangled states with a fixed photon number N at the input, which is a common practical task, considering the simplest type of click detectors that cannot resolve the number of arriving photons, and cannot distinguish the photon polarization state. Notably, the state characterization can also be generalized to the regime when the maximum photon number is known. If no more than one photon arrives at such a detector positioned at the diffraction order m, then its response is governed by the following POVM operator,

$$\hat{A}^{(m)} = \sum_{p=H,V} \hat{b}_{m,p}^{\dagger}\hat{b}_{m,p} = \sum_{p,p'=H,V} A_{p,p'}^{(m)}\, \hat{a}_p^{\dagger}\hat{a}_{p'} \ , \quad (4)$$

and we calculate the matrix expression

$$\mathbf{A}^{(m)} = \left(\mathbf{T}^{(m)}\right)^{\dagger}\mathbf{T}^{(m)} = \sum_{j=1,2} s_{m,j} \left|W_j^{(m)}\right\rangle\left\langle W_j^{(m)}\right| = (s_{m,1} - s_{m,2}) \left|W_1^{(m)}\right\rangle\left\langle W_1^{(m)}\right| + s_{m,2} I \, .$$

We see that this is a sum of a polarization projection operator and a polarization-insensitive detection. The presence of the latter term is a consequence of the partial-polarizer transformation at each of the diffraction orders. Although conventional polarimetry requires near-perfect polarizers (i.e. $s_{m,2} = 0$), we find that POVM formalism enables unique and accurate quantum state reconstruction in the regime of $s_{m,2} > 0$.

After determining the detection operators, we find the probabilities of the simultaneous detection of N photons by a combination of N detectors at the diffraction orders $m_1, m_2, \dots, m_N$, when there is exactly one photon at each detector. These are proportional to the corresponding photon correlations:

$$\Gamma(m_1, m_2, \dots, m_N) = \mathrm{Tr}(\rho_N \hat{A}_{m_1}\hat{A}_{m_2}\cdots\hat{A}_{m_N}).$$

Here, ρ_N is an input density matrix. Then, we follow an established procedure [21, 20] to enumerate with index q all the possible N combinations of M detectors, $(m_1, m_2, \dots, m_N)$ and rewrite Eq. (6) in an equivalent form,

$$\Gamma_q = \sum_{s=1}^{S} B_{p,s} r_s \ .$$

Here r_s are the independent real and imaginary parts of the input density matrix, $S = (N+3)!/(3!\,N!)$, $q = 1, \dots, Q$, $Q = M!/(N!\,(M-N)!)$, and M is the total number of detected diffraction orders. The matrix elements $B_{p,s}$ depend on the transfer matrix elements, and more specifically on the

vectors $W_j^{(m)}$ and singular values $s_{m,p}$.

We can then reconstruct an input state from the correlation measurements by performing a pseudo-inversion, provided the number of different correlations matches or exceeds the number of unknowns, $Q \geq S$,

$$M \geq N + 3 \ .$$

Importantly, in addition to the necessary condition, it is essential that reconstruction results are robust in presence of experimental errors in the correlation measurements. This can be expressed as a requirement to minimize the condition number κ of matrix B, defined as a ratio of its largest and smallest singular values

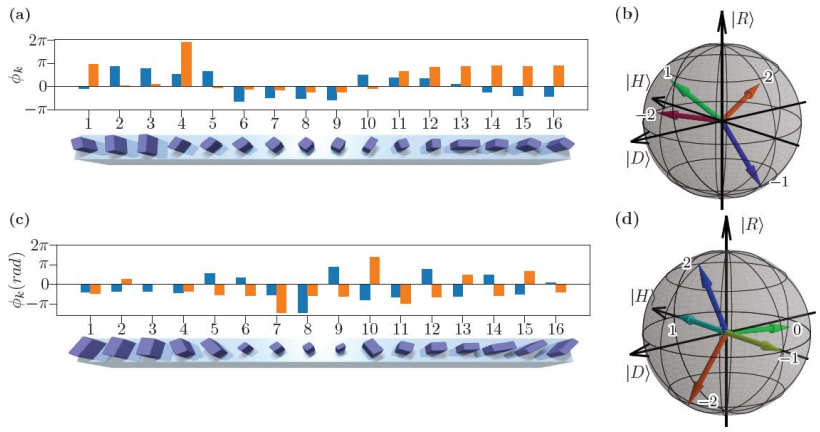

Figure 3.2: (a) Ordinary and extra ordinary phase retardances (ϕ_o, ϕ_e) for a metasurface numerically optimized for polarimetry of a single incoming photon state. The render shows the metasurface calculated via analytical calculations and Rigorous Coupled Wave Analysis (RCWA), including the angles to which each element is rotated. The metasurface was designed as $832nm$ thick amorphous silicon on glass, and has an inverse condition number $1/\kappa = 0.573$, close to the theoretical limit of $1/\sqrt{2}$. (b) Poincaré sphere representation of partially polarized diffraction orders $(\pm 2, \pm 1)$ used as the basis states to affect the single-shot polarimetry using the metasurface shown in (a). (c) Phase retardances and three-dimensional render of a metasurface designed for polarimetry of an incoming bi-photon state, simulated for $790nm$ thick amorphous silicon on glass. This has an inverse condition number of 0.170. (d) Basis states for $(\pm 2, \pm 1, 0)$ single-shot polarimetry of bi-photon states.

The metasurface was designed and optimized in multiple steps. First, multi-stage optimization of the metagrating's phase parameters was performed via a semi-analytical approach, targeting the most robust polarization reconstruction using the inverse condition number. Knowing that each cuboidal resonator defines a transfer matrix $\mathbf{U}$ represented in the Jones formalism as

$$\mathbf{U} = \mathbf{R}(-\theta).\begin{bmatrix} e^{i\phi_o} & 0 \\ 0 & e^{i\phi_e} \end{bmatrix}.\mathbf{R}(\theta) \quad (9)$$

where $\mathbf{R}(\theta)$ is a two-by-two rotation matrix by angle θ and ϕ_o and ϕ_e are the phase shifts imposed by the resonator along the ordinary and extraordinary axis, we defined a metagrating as the action of some number of pixels arranged into a periodic supercell, as shown in Fig. 3.2(a,c). It is therefore possible to analytically calculate the transformation matrix of the metasurface using the fourier transform.

$$\mathbf{T}^{(m)} = \sum_{j=0}^{N} \mathbf{U}^{(j)} e^{-\frac{2\pi i}{N} mn}, (10)$$

where N is the total number of elements in a single unit cell, each of which has a transfer matrix $\mathbf{U}^{(j)}$. This was implemented numerically using a fast fourier transform, thus allowing for the calculation of the condition number κ as the ratios of the minimum and maximum singular value decomposition values. By minimizing the condition number, it is thus possible to optimize towards a highly robust design. This optimization produced a set of phase parameters corresponding to each pixel of the unit cell, consisting of phase-shifts along the ordinary and extraordinary axes of each pixel as well as the angle of each pixel, which may be seen in 3.2(a,c) for one- and two-photon designs respectively. This

also allowed us to calculate the basis states of the diffraction orders to be used for the reconstruction, demonstrating that they are clearly non-orthogonal.

The vectors $\mathbf{W}_j^{(m)}$ are the basis states of the projection measurement. By converting these to a Stokes basis, these may be plotted on a Poincaré sphere for convenient visualization of the basis states implemented by a given metasurface design, as shown in Fig. 3.2(b, d), with the lengths normalized as

$$R = 1 - \frac{P_{min}}{P_{max}},$$

where P_{min} and P_{max} are the minimum and maximum powers transmitted to the relevant diffraction order. Furthermore, this provides a convenient conversion between the Jones transfer matrix formalism and the instrument matrix formalism: The vector components of the instrument matrix ($In_1^{(m)}$, $In_2^{(m)}$, $In_3^{(m)}$) are exactly equivalent to the basis state vector as derived from $\mathbf{W}_j^{(m)}$.

A physical parameter sweep of cuboidal pixels was then computed using a numerical technique known as Rigorous Coupled Wave Analysis (RCWA), thus producing a phase map from which suitable designs could be selected analytically. The physical parameters of the metasurface were thus designed by selecting pixels from the sweep that fit desired phase parameters, up to an arbitrary global phase, while accounting for the rotations of the pixels. This thus greatly simplifies the design process, reducing the parameters considered to just the length and widths of the cuboidal pixels. The combined metasurface structure thus designed was then simulated using a commercial electrodynamics solver, CST Studio, as a final optimization pass and safeguard against second and higher order interactions between adjacent pixels that are not accounted for in the analytical design.

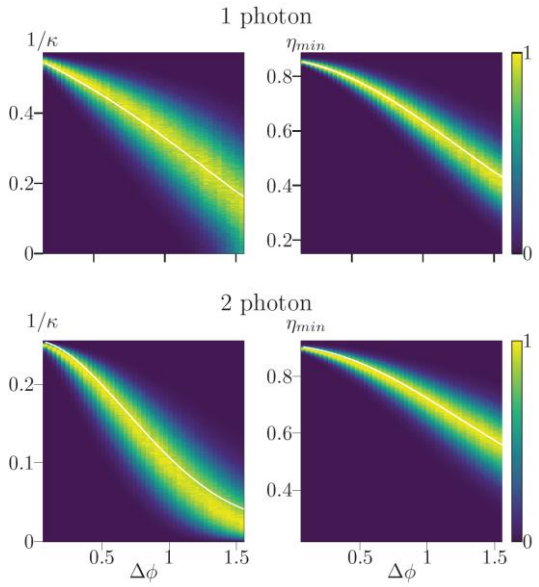

Figure 3.3: Plots demonstrating the resistance to random fabrication error $\Delta\phi$ of the single and double photon metasurface designs. The numerically calculated designs were perturbed by adding random errors up to a maximum of $\Delta\phi$ to each of the nanoresonator elements, and the inverse condition numbers $1/\kappa$ and diffraction efficiencies η_{min}, defined as the minimum power that is captured within the diffraction orders used. The errors were randomized 100000 times for each value of $\Delta\phi$, and the results normalized at each value to a total probability of 1.

Based on the POVM formulation of the design, strong robustness against fabrication errors is expected of the metasurface. Numerical simulations were carried out to demonstrate this. Using the analytical design of a metasurface designed for single- and double- photons, random errors were introduced as follows.

Under realistic fabrication scenarios, the most common deviations from the analytical design pertain to

the overall sizes of the nanoresonators. This were modelled as variance in the phase shifts along the ordinary and extraordinary axes of the individual nanopixels, i.e. random errors up to $\delta\phi$ were added to each nanopixel, and the overall transmission of the altered metasurface structure calculated via superposition of the electric fields and subsequent fourier transformation. From this result, we computed the overall inverse condition number for the altered metasurface. By trialing large numbers of errors, we estimated the falloff of performance with the degree of random error, as shown in Fig. 3.3. The errors trialed range up to an extreme case of $\Delta\phi = \pi/2$, which may be considered to be well in excess of accuracy of nanofabrication technology.

We find that for realistic levels of error, on the order of 10^{-1}, both the inverse condition number and the diffraction efficiencies do not drop significantly, as shown in Fig. 3.3. However, as one might expect, the double-photon design is more sensitive to error than the single-photon design, owing to the necessary consideration of additional diffraction orders to fully resolve multiple photons.

The metasurfaces were fabricated [Fig. 3.4(b)] from a $832nm$-thick amorphous silicon layer prepared at the ANU node of Australian Nanofabrication Facility (ANFF) using Plasma-Enhanced Chemical Vapor Deposition (PECVD) on a glass substrate. It was subsequently etched at the University of Jena using Electron Beam Lithography (EBL) and Inductively Coupled Plasma (ICP) etching. Slight variants in the prepared metasurfaces were prepared by in turn varying the EBL exposure times, accounting for minor errors due to fabrication error.

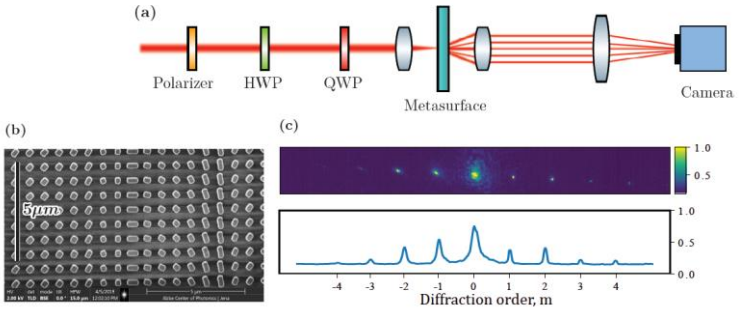

Figure 3.4: (a) Schematic of the experimental setup used to classically characterize the metasurface. Input states were prepared from a variable-wavelength infrared laser using a fixed polarizer and motorized half- and quarter- waveplates, before being collimated on the metasurface by lenses. Output diffraction order intensities were collected using a CCD camera. (b) Scanning Electron Microscope (SEM) image of the metasurface, fabricated as $832nm$ amorphous silicon on glass via electron beam lithography. (c) Representative reading as taken using the camera, and the processed intensity plot obtained by slicing across the diffraction orders. Intensities were normalized to 1.

After fabrication, the metasurfaces were characterized using the experimental setup shown in Fig. 3.4(a). The experiment was performed fully in free-space. Using a half waveplate, quarter waveplate and fixed polarizer, polarization states were prepared from a variable-wavelength laser operating in the $1500 - 1575nm$ telecommunications bandwidth. The prepared polarization state was then focused to a spotsize of approximately $1\mu m$ normally incident on the metasurface. The diffraction orders were then collected using an objective lens with a high numerical aperture, and further focused onto an infrared CCD camera using a convex lens. As a separate measurement, the camera was replaced with a calibrated power meter in order to determine the total power that was transmitted through the metasurface.

The intensities of the diffraction orders over varying input polarization orders were thus captured as images in the camera, as shown in Fig. 3.4(c). The diffraction order spot locations were determined by hand, and the individual intensities were extracted by integrating the total intensities around each location. Each diffraction order was then fitted individually. We thus characterized the instrument matrix of the metasurface as a $4 \times m$ matrix. By normalizing this according to the degenerate elements of the density matrix, we may calculate the N-photon inverse condition number of the reconstruction.

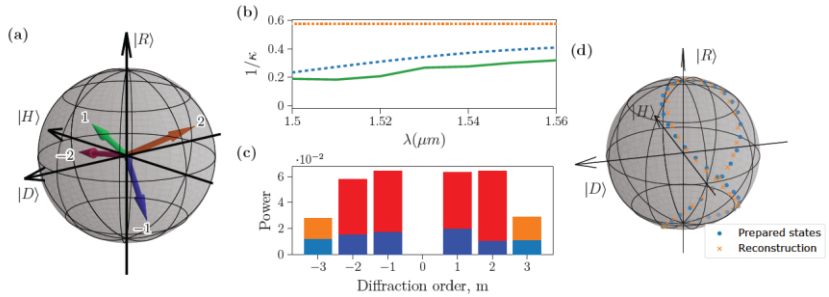

Figure 3.5: (a) Poincaré sphere representation of the basis states as calculated from the $(\pm 2, \pm 1)$ diffraction orders of the fabricated metasurface. These are, as predicted, partially polarized states. (b) The experimentally characterized inverse condition numbers of the metasurface across a wavelength range are plotted using the solid green line. The blue, dashed line represents the original RCWA design target, and the orange, dotted line represents the theoretical maximum. (c) The minimum and maximum power directed to each diffraction order, as determined by experiment. (d) Poincaré sphere showing a comparison of input states versus the reconstructed states using the experimentally characterized metasurface.

From this characterization, we compute first the polarization bases of the instrument matrix, and plot a representative example in Fig. 3.5(a), calculated at a wavelength of at $1560nm$. We further computed and plotted the inverse condition number across the wavelengths, along with the inverse condition number from the numerical design [Fig. 3.5(b)]. The experimentally calibrated inverse condition number deviates from the design target only by up to 15%.

From the experimental data as well as the instrument matrix of the metasurface, a reconstruction was performed. From experimental data, an arbitrary range of angles for the half- and quarter- waveplates were chosen. From these angles, and knowing that the first polarizer was positioned vertically, we thus know the polarization states $\psi_{in}^{(m)}$ before incidence on the metasurface, accounting for experimental angular misalignment. For these input states, we also compute the states reconstructed from the measured intensities P_{out} and the experimentally characterized instrument matrix In, as:

$$\psi_{recon}^{(m)} = In^{-1}.P_{out}$$

We then plotted these on the same Poincaré sphere for comparison, as shown in Fig. 5(d), and thus demonstrate that the reconstruction is successful with high accuracy.

4) Optimal Monitoring of Deviations from Target Polarization with Metasurfaces, Ref. [3]

We show the concept of the metasurface enabled sensitive monitoring of polarization deviations in Fig. 4.1. An elliptical polarization shown by the black spot on the Poincaré sphere in Fig. 4.1(a) and defined by $|\Psi\rangle$ is an arbitrarily chosen anchor polarization state. The quantity that needs to be sensed alters the anchor polarization by a small deviation δ, bringing it to the perturbed input state $|\Psi_{\text{in}}\rangle = |\Psi\rangle + \delta|\widetilde{\Psi}\rangle$, where $|\widetilde{\Psi}\rangle$ represents the orthogonal polarization of $|\Psi\rangle$, i.e. $\langle\widetilde{\Psi}|\Psi\rangle = 0$. The size of the red spherical area near the anchor polarization state indicates the magnitude of the deviation. It is hard to directly monitor such a small polarization deviation when $|\delta| \ll 1$, which would require a polarimeter with extremely high resolution. A polarimeter typically comprises of several optical elements and requires multiple measurements, which are always prone to errors and thus have limited resolution. We develop a novel concept of using a metasurface to project the anchor polarization $|\Psi\rangle$ to a linear polarization state with attenuated power, while the small deviation $\delta|\widetilde{\Psi}\rangle$ is almost fully mapped to the orthogonal linear polarization state. By doing so the initial deviation δ is magnified and becomes easily detectable in the form of linear polarizations, whose monitoring requires only a single linear polarization splitter and two detectors.

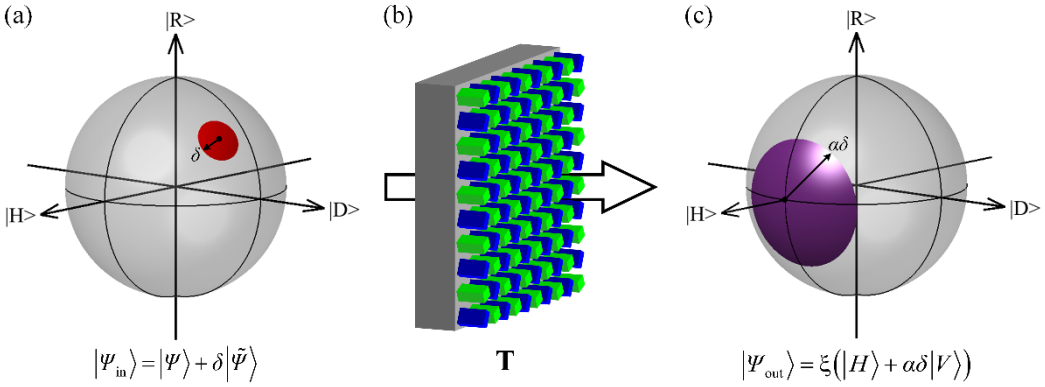

Fig. 4.1. Concept of sensitive polarization deviation monitoring with metasurfaces. (a) An arbitrarily chosen elliptical anchor polarization shown by a black dot on a Poincaré sphere and deviations up to $|\delta|$ are indicated by red spherical crown. (b) A metasurface performing a special non-conservative transformation **T**. (c) The transmitted anchor state is converted to a horizontal polarization, with the vertical component representing amplified responsivity to deviations by a factor α.

We design a metasurface that realizes a transformation **T** [Fig. 4.1(b)] according to the following principles. First, it converts the input anchor polarization to the $|H\rangle$ state, such that the output $|V\rangle$ component is zero in absence of perturbations. Then, the deviations are associated with the appearance of the output vertical polarization component, see Fig. 4.1(c). The corresponding deviation amplitude which is the ratio of the V-H amplitudes is $\eta = |\langle V|\mathbf{T}|\Psi_{\text{in}}\rangle / \langle H|\mathbf{T}|\Psi_{\text{in}}\rangle|$. Accordingly, the second metasurface design goal is to increase the deviations by a factor α, such that the ratio of output vertical and horizontal components provides an amplified value of the deviation. Such conditions can be only satisfied by a *non-unitary* polarization transformation **T** expressed as

$$\mathbf{T} = \xi\left(|H\rangle\langle\Psi| + \gamma|H\rangle\langle\tilde{\Psi}| + \alpha|V\rangle\langle\tilde{\Psi}|\right). \qquad (1)$$

We define the amplification of the output V-H power ratio over the input perturbation-anchor power ratio as the *responsivity* of this scheme, that is $S = |\eta|^2/|\delta|^2$. For small perturbations with $|\delta| \ll 1$, $|\Psi_{\text{out}}\rangle \simeq \xi(|H\rangle + \alpha\delta|\text{V}\rangle)$ and thus $\eta \simeq |\alpha\delta|$ and $S \simeq |\alpha|^2$. For a specific anchor polarization state $|\Psi\rangle$ = [cos(β), sin(β)exp(iφ)]$^{\text{T}}$, we analytically determine the *optimal metasurface* transformation by identifying the two scaling parameters ξ, γ which maximize the mapping of deviations to the $|V\rangle$ component, under the constraints of (i) a chosen responsivity S_0 and (ii) a passive (non-amplifying) and non-chiral (symmetrical) **T**. The optimal transformation has the following form

$$\mathbf{T} = \frac{1}{\sigma_m}\mathbf{T}_0 = \frac{1}{\sigma_m}\begin{bmatrix} \frac{1/\sqrt{S_0} - \sin^2(\beta)}{\cos(\beta)}\exp(i\varphi) & \sin(\beta) \\ \sin(\beta) & -\cos(\beta)\exp(-i\varphi) \end{bmatrix} \qquad (2)$$

where σ_m is the maximum singular value of $\mathbf{T}_0$.

We achieve the optimal transformation **T** with a monolithic dielectic metasurface by non-trivially generalizing the use of pairwise structures, which we have developed for synthesizing the polarization-dependent diffraction loss [1]. An exemplary metasurface layout is shown in Fig. 2(a) with a unit cell consisting of two types of silicon nano-pillars, each realizing a unitary transformation $\mathbf{U_1}(\phi_e^{(1)}, \phi_o^{(1)}, \theta^{(1)})$ or $\mathbf{U_2}(\phi_e^{(2)}, \phi_o^{(2)}, \theta^{(2)})$, such that for the whole metasurface $\mathbf{T} = (\mathbf{U_1} + \mathbf{U_2})/2$. This structure enables amplified sensing of polarization deviations around the non-trivial elliptical polarization state sketched in Fig. 2(b), with $|\Psi\rangle = [\cos(0.2\pi), \sin(0.2\pi)\exp(0.3i)]^{\text{T}}$. We also plot a perturbed state $|\Psi_{\text{in}}\rangle$ with a dashed ellipse, corresponding to $|\delta| = 0.1$. The optimal design parameters of nano-resonators, the orientation angles $\theta^{(1,2)}$ and the phase retardances $\phi_{o,e}^{(1,2)}$ along the two axes labeled ordinary (o) and extraordinary (e), nontrivially depend on the amplitude ratio enhancement parameter α, see Fig. 4.2(c). In Fig. 4.2(d) we plot the dependence of the V-H amplitude ratio readout η on the perturbation strength $|\delta|$ for two representative values of target amplification factor $\alpha = 2, 10$. We observe that transformations with larger α exhibit more pronounced enhancement of V-H ratio for a large range of polarization perturbations. According to the original aim, the largest amplification of deviations occurs in the range of small $|\delta|$, which can facilitate the monitoring of weak perturbations.

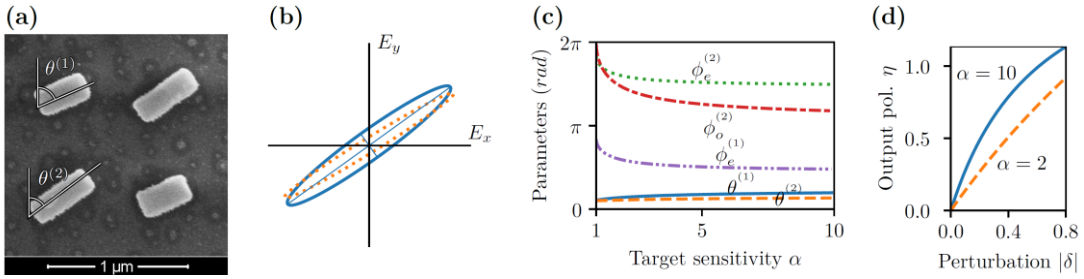

Fig. 4.2. Realization of optimal metasurfaces for monitoring of polarization deviations. (a) Scanning electron microscope (SEM) image of a fabricated metasurface designed to resolve an anchor polarization state $|\Psi\rangle = [\cos(0.2\pi), \sin(0.2\pi)\exp(0.3i)]^{\mathrm{T}}$ with the target amplification $\alpha = 10$. (b) The elliptical anchor polarization $|\Psi\rangle$ (solid), and a perturbed state $|\Psi_{\mathrm{in}}\rangle$ with $|\delta| = 0.1$ (dashed). (c) Optimal nanoresonator orientations and phase retardance (with $\phi_o^{(1)} = 0$) vs. the target sensitivity α. (d) The output V-H ratio η vs. the perturbation magnitude $|\delta|$ for the amplifications $\alpha = 2, 10$.

Results, Discussion, Plans for Next Option Period: Describe significant experimental and/or theoretical research advances or findings and their significance to the field. Describe the main objectives for the next year.

The **key results** are as follows:
1) Development of metasurfaces that can perform arbitrary transformation of polarization photon pairs, Ref. [1].

Birefringent materials or nanostructures that introduce phase differences between two linear polarizations underpin the operation of wave plates for polarization control of light. Here we develop metasurfaces realizing a distinct class of complex-birefringent wave plates, which combine polarization transformation with a judiciously tailored polarization-dependent phase retardance and amplitude filtering via diffraction. We prove that the presence of loss enables the mapping from any chosen generally non-orthogonal pair of polarizations to any other pair at the output. We establish an optimal theoretical design-framework based on pairwise nanoresonator structures and experimentally demonstrate unique properties of metasurfaces in the amplification of small polarization differences and polarization coupling with unconventional phase control. Furthermore, we reveal that these metasurfaces can perform arbitrary transformations of biphoton polarization-encoded quantum states, including the modification of the degree of entanglement. Thereby, such flat devices can facilitate novel types of multi-functional polarization optics for classical and quantum applications.

2) Discerning Polarization Objects using Quantum Non-local Measurements with Metasurfaces, Ref. [4].

We developed theoretically a generalized scheme to discern polarization-sensitive objects and their rotation through non-local measurements using non-classical light. Remarkably, we proved that non-classical correlations between probe and reference-photons are needed to enable discrimination of all types of objects. Our proposed measurement scheme can be implemented with dielectric metasurfaces that harness modern advanced nanofabrication capabilities for high-fidelity operation. We believe, that this approach can satisfy the strong demand in research and industry for efficient and integrated optical schemes performing characterization of objects with polarization-sensitive transmission characteristics across a broad spectral range. In particular, it can benefit applications demanding accurate discrimination of objects with various polarization characteristics, including sets of phase objects like biological samples.

3) Single Metagrating for Multi-Photon Polarization Measurements, Ref. [11].

We formulated a new conceptual approach for one-shot full Stokes polarization measurement with a single metagrating, and develop novel design through advanced computational optimization of individual nano-resonator properties delivering robust operation even under strong fabrication inaccuracy. We fabricated the metasurface from amorphous silicon nanostructures deposited on glass,

and experimentally confirmed accurate optical polarization reconstruction. We anticipate that our new concept will facilitate diverse applications such as optimal polarization state imaging tailored for computer vision or quantum state characterization.

4) Optimal Monitoring of Deviations from Target Polarization with Metasurfaces, Ref. [3]

We reveal that non-chiral dielectric metasurfaces can provide amplified responsivity for monitoring small deviations in the vicinity of an arbitrarily chosen anchor polarization state through a simple readout of output horizontal and vertical components. We determine the analytically optimal design and its practical realization through a binary combination of nanoresonators with tailored characteristics. We anticipate that our work will enable a new class of ultra-compact and ultra-sensitive flat meta-optical devices for a broad range of applications, including advanced sensing, imaging, and metrology in both classical and quantum photonics.

Plans for Next Option Period

Option plan

Aim: Develop multi-functional metasurfaces for in-line quantum state monitoring and transformation.

Conceptual approach: Develop a next generation of metasurfaces for realization of in-line monitoring of quantum photon states, based on detection of a small fraction of photons. The transmitted photons will be left either undisturbed, or transformed up to the required specifications. For this purpose, we will build on the results achieved in Year 1, to realize the multi-functional metasurfaces addressing a range of needs in quantum optical communications.

Work plan and methodology:
Our working principle is to design a metasurface which splits only a small fraction of light to diffraction orders, while at the same time transmitting most of the photons in the forward direction. We will build on our recently formulated general theoretical framework of in-line quantum state monitoring and employ advanced machine learning approaches to develop most efficient and robust metasurface design to simultaneously (i) apply a desired quantum polarization state transformation to the transmitted photons and (ii) realize effective POVM operators at different diffraction orders enabling state monitoring and discrimination (QSD). Thereby, such metasurfaces would be capable of integrating the multiple different functionalities, providing a key step forward compared to single-function optimized metasurfaces targeted in Year 1, opening up completely new opportunities for applications.

List of Publications and any Significant Collaborations that resulted from your AOARD supported project: In standard format showing authors, title, journal, issue, pages, and date, for each category list the following:
a) papers published in peer-reviewed journals,

1. S. Lung, K. Wang, K. Zangeneh Kamali, J. Zhang, M. Rahmani, D. N. Neshev, A. A. Sukhorukov,
   "Complex-birefringent dielectric metasurfaces for arbitrary polarization-pair transformations,"
   ACS Photonics **7**, 3015–3022 (2020), https://doi.org/10.1021/acsphotonics.0c01044

b) papers published in peer-reviewed conference proceedings,

2. S. Lung, K. Wang, K. Zangeneh Kamali, M. Rahmani, D. N. Neshev, A. A. Sukhorukov,
   "Arbitrary Transformation of Two-Photon Polarization-Entangled States with Metasurfaces,"
   14th Pacific Rim Conference on Lasers and Electro-Optics (CLEO PR 2020), OSA Technical Digest, paper C7C_1 (2020), https://doi.org/10.1364/CLEOPR.2020.C7C_1
3. S. Lung, J. Zhang, K. Wang, K. Zangeneh Kamali, M. Rahmani, D. N. Neshev, A. A. Sukhorukov,
   "Optimal Monitoring of Deviations from Target Polarization with Metasurfaces,"

14th Pacific Rim Conference on Lasers and Electro-Optics (CLEO PR 2020), OSA Technical Digest, paper C2E_2 (2020), https://doi.org/10.1364/CLEOPR.2020.C2E_2

4. A. Vega, K. Wang, S. Lung, D. E. Jones, M. Brodsky, T. Pertsch, F. Setzpfandt, A. A. Sukhorukov,
"Discerning Polarization Objects using Non-local Measurements with Metasurfaces,"
Conference on Lasers and Electro-Optics (CLEO 2020), OSA Technical Digest, paper FM1C.7 (2020), https://doi.org/10.1364/CLEO_QELS.2020.FM1C.7
5. S. Lung, K. Wang, K. Zangeneh Kamali, M. Rahmani, D. N. Neshev, A. A. Sukhorukov,
"Optimal Monitoring of Deviations from Target Polarization with Metasurfaces,"
Conference on Lasers and Electro-Optics (CLEO 2020), OSA Technical Digest, paper FM4B.6 (2020), https://doi.org/10.1364/CLEO_QELS.2020.FM4B.6
6. (Invited) A. A. Sukhorukov,
"Manipulating and Imaging Quantum Light with Dielectric Metasurfaces,"
OSA Advanced Photonics Congress (AP 2019), OSA Technical Digest, paper NoT3B.2 (2019), https://doi.org/10.1364/NOMA.2019.NoT3B.2

c) papers published in non-peer-reviewed journals and conference proceedings,
d) conference presentations without papers,

8. (Invited) A. A. Sukhorukov, "*Quantum and classical nonconservative photonics with dielectric metasurfaces*," METANANO – International Conference on Metamaterials and Nanophotonics, 14-18 September 2020, St. Petersburg, Russia, Online.
9. S. Lung, J. Zhang, K. Wang, K. Zangeneh Kamali, M. Rahmani, D. N. Neshev, A. A. Sukhorukov, "*Optimal Monitoring of Small Polarization Perturbations with Metasurfaces*," Metamaterials 2020 - 14th International Congress on Artificial Materials for Novel Wave Phenomena, 28 September – 3 October 2020, New York, USA, Online.
10. (Invited) A. A. Sukhorukov, "Generation and shaping of quantum photon-pair states in nonlinear metasurfaces," SPIE Optics and Photonics: Advances in Photonics, 23-27 August 2020, San Diego, USA, Online.
11. S. Lung, N.R.H. Pedersen, K. Wang, K. Zangeneh Kamali, F. Setzpfandt, A. A. Sukhorukov, "*Optical Metagrating for One-Shot Polarization Measurements*," Australian and New Zealand Conference on Optics and Photonics (ANZCOP), paper 11201-37, 8-12 December 2019, Melbourne, Australia.
12. (Invited) A. A. Sukhorukov, "*Interaction of quantum states of light with metasurfaces*," Metamaterials 2019 - 13th International Congress on Artificial Materials for Novel Wave Phenomena, 16-21 September 2019, Rome, Italy.
13. (Invited) A. A. Sukhorukov, "*Shaping of quantum states of light with metasurfaces*," International Conference of Nonlinear, Quantum and Nanophotonics (ICNQN 2019), 2-4 September 2019, Sofia, Bulgaria.
14. (Invited) A. A. Sukhorukov, "*Non-Hermitian transformations with optical metasurfaces*," META19 - the 10th International Conference on Metamaterials, Photonic Crystals and Plasmonics, 23-26 July 2019, Lisbon, Portugal.

e) manuscripts submitted but not yet published, and
The following manuscripts are fully prepared and are at the stage of final editing and proof-reading before submission:

14. S. Lung, N.R.H. Pedersen, K. Wang, K. Zangeneh Kamali, F. Setzpfandt, A. A. Sukhorukov,
"Single Metagrating for Multi-Photon Polarization Measurements"
15. A. Vega, T. Pertsch, F. Setzpfandt, A. A. Sukhorukov, "*Non-local Identification of Polarization-sensitive Objects using Metasurfaces*"

f) provide a list any interactions with industry or with Air Force Research Laboratory scientists or significant collaborations that resulted from this work.

1) The project supported collaboration with Dr. Michael Brodsky, a group leader at U.S. Army Research Laboratory, Adelphi, USA. We have jointly developed a concept of polarization monitoring with entangled photons [4], and plan its further application for monitoring quantum photon transmission in fiber communication lines.

2) We have developed collaboration on the subject of quantum measurements with dielectric metasurfaces with Dr. Frank Setzpfandt at Jena University [4, 11]. We were recently awarded an ANU-DAAD travel exchange grant over 2021-2022 for students and early-career researchers to work on joint experiments and develop links with German industry.

Attachments: Publications a), b) and c) listed above if possible.

Important Note: If the work has been adequately described in refereed publications, submit an abstract as described above and refer the reader to your above List of Publications for details. If a full report needs to be written, then submission of a final report that is very similar to a full length journal article will be sufficient in most cases. This document may be as long or as short as needed to give a fair account of the work performed during the period of performance. There will be variations depending on the scope of the work.